Harnessing icIEF to Unlock Protein-Based Therapeutics

Read the new Article Collection

Harnessing icIEF to Unlock Protein-Based Therapeutics

ARTICLE COLLECTION

WILEY Analytical Science

Sponsored by:
bio-techne proteinsimple

Keep up to date with the latest developments in biotherapeutics and the range of treatments for various diseases with our latest article collection. Find out how imaged cIEF (icIEF) technique is essential for quality control and analytical development of these drugs, as it accurately determines the surface charge of lipid nanoparticles and the charge heterogeneity of proteins and antibodies.

This article collection aims to provide you with more information on these techniques and technologies, helping you further your research in this field.

bio-techne | proteinsimple

WILEY

Biotechnology
Journal

RESEARCH ARTICLE

Mini- and macro-scale direct perfusion bioreactors with optimized flow for engineering 3D tissues

Gordian Born[1] | Evelia Plantier[2] | Guido Nannini[3] | Alessandro Caimi[3] |
Andrea Mazzoleni[1] | M. Adelaide Asnaghi[2] | Manuele G. Muraro[2] |
Arnaud Scherberich[1,2] | Ivan Martin[1,2] | Andrés García-García[2] 🔘

[1]Department of Biomedical Engineering, University of Basel, Basel, Switzerland

[2]Department of Biomedicine, University Hospital Basel, University of Basel, Basel, Switzerland

[3]Department of Electronics, Informatics and Bioengineering (DEIB), Politecnico di Milano, Milan, MI, Italy

Correspondence
Ivan Martin, Department of Biomedicine, University Hospital Basel, University of Basel, 4031 Basel, Switzerland.
Email: ivan.martin@usb.ch

Abstract

Bioreactors enabling direct perfusion of cell suspensions or culture media through the pores of 3D scaffolds have long been used in tissue engineering to improve cell seeding efficiency as well as uniformity of cell distribution and tissue development. A macro-scale U-shaped bioreactor for cell culture under perfusion (U-CUP) has been previously developed. In that system, the geometry of the perfusion chamber results in rather uniform flow through most of the scaffold volume, but not in the peripheral regions. Here, the design of the perfusion chamber has been optimized to provide a more homogenous perfusion flow through the scaffold. Then, the design of this macro-scale flow-optimized perfusion bioreactor (macro-Flopper) has been miniaturized to create a mini-scale device (mini-Flopper) compatible with medium-throughput assays. Computational fluid dynamic (CFD) modeling of the new chamber design, including a porous scaffold structure, revealed that Flopper bioreactors provide highly homogenous flow speed, pressure, and shear stress. Finally, a proof-of-principle of the functionality of the Flopper systems by engineering endothelialized stromal tissues using human adipose tissue-derived stromal vascular fraction (SVF) cells has been offered. Preliminary evidence showing that flow optimization improves cell maintenance in the engineered tissues will have to be confirmed in future studies. In summary, two bioreactor models with optimized perfusion flow and complementary sizes have been proposed that might be exploited to engineer homogenous tissues and, in the case of the mini-Flopper, for drug testing assays with a limited amount of biological material.

KEYWORDS
bioreactor, perfusion flow, tissue engineering

Ivan Martin and Andrés García-García contributed equally to this study.

- -

1 | INTRODUCTION

Direct perfusion bioreactors used in tissue engineering approaches rely on convective transport to push a liquid phase (e.g., cell suspension and/or medium) through the pores of three-dimensional (3D) scaffolds or the interstitial tissue space. In comparison to static cultures, direct perfusion flow offers several advantages to engineer in vitro 3D tissues. For example, it increases cell seeding efficiency on the scaffolds, facilitates the transfer of oxygen, nutrients, and waste products to and from the cells, and exposes the forming tissue to physiological-like shear stress.[1,2]

We previously designed and validated a macro-scale perfusion bioreactor that enhances the seeding efficiency and uniformity of different mesenchymal cell types in 3D scaffolds.[3,4] In the last two decades, this system (hereafter referred to as U-CUP; U-shaped bioreactor for cell culture under perfusion, Cellec Biotek AG) has been applied to engineer and/or culture in vitro different macro-scale tissues such as osteogenic and vasculogenic grafts,[5–9] cartilaginous grafts,[10,11] bone marrow,[12–15] colorectal cancer,[16,17] muscle,[18] breast cancer,[19,20] pericardium,[21,22] periodontal pocket,[23] fat,[24] meninges,[25] and thymus.[26] However, the acute expansions in the rectangular geometry of the U-CUP flow chamber might cause nonuniform flow speed areas in the periphery of the scaffold.[27] Furthermore, from the size perspective, the dimensions of this bioreactor (35 cm high, 5 cm deep, and 10 cm wide) and the volume of medium required (normally 8 ml per bioreactor) limit its use in medium-throughput assays to culture tiny biopsies in the context of precision medicine.[17,19]

Here, we first revised the U-CUP **macro**-scale bioreactor by engineering a new chamber design to provide **Fl**ow-**op**timized **per**fusion (macro-Flopper) through the scaffold. Next, we miniaturized the design of the macro-Flopper to create a mini-scale bioreactor (mini-Flopper). Finally, we aimed at providing a first proof-of-principle of the functionality of these new bioreactor models by engineering endothelialized stromal tissues, previously referred to as "angiogenic niches"[9] using human adipose tissue-derived stromal vascular fraction (SVF) cells seeded on collagen-based scaffolds.

2 | EXPERIMENTAL SECTION

2.1 | Design of the macro-scale flow-optimized perfusion bioreactor (macro-Flopper)

The macro-Flopper bioreactor was similar to the U-CUP system except for the perfusion chamber (**Figure 1A**, colored in brown, and Figure S1, Supporting Information). In the inner part of the U-CUP chamber, there was an URD08H04 adapter (cup holding the scaffold) and two ETFE grids, leaving a scaffold space of 8×3 mm (diameter × height). In the inner part of the macro-Flopper perfusion chamber, the adapter (from here referred as cup) was made of two assembled silicone parts (Figure 1B; upper in red and bottom in blue) with integrated ETFE grids (Figure 1B; white), also generating a scaffold space of 8×3 mm (diam-

eter × height). A two-components shell formed the outer part of the perfusion chamber to keep the silicone cup under pressure, ensuring sealing and sterility of the culture environment (Figure 1C–D). In both bioreactor systems, the closure of the chamber induced a compression of the scaffold to reach a final size of 8×2 mm (diameter × height).

The chamber was connected to the tubing through three-way valves and ULN 1/4″–28 threadings. The top and bottom parts of the cup in the macro-Flopper were made by pouring silicone in polylactic acid (PLA) 3D-printed molds (upper part, Figure 1E; bottom part, Figure 1F) with glued ETFE grids (SEFAR Fluortex #09-590/47; white in Figure 2E,F). Once the silicone was cured, the cup parts were washed in water and ready to use. Blender 2.82 was used to design and generate the .stl files, Cura 4.6 was used to generate the Gcode. An Anycubic mega 3D printer was used to print the molds in PLA with a wall/bottom/top thickness of 2 mm and an infill of 20% with a step size of 100 μm. The shell parts of the macro-Floppers were designed, and STEP files were sent to the company Xometry (https://xometry.eu/de/) to be machined using polyether ether ketone (PEEK).

2.2 | Design of miniaturized flow-optimized perfusion bioreactor (mini-Flopper)

The mini-Flopper bioreactor (Figure 2A) was designed to fulfill the following requirements: modular, autoclavable, compatible with sample sizes of 6–113 mm³ (2–4-mm diameter and 3–36-mm high) and medium volumes of 750 μl–3 ml, and easy to operate under sterile conditions (Figure S1, Supplementary Information). The core consisted of three main parts (upper, middle, and bottom parts; Figure 2B–D) fixed with connectors, hinges, and clippers (Figure 2E–G), in which 4-mm-round steel rods were inserted as hinge pins (Figure 2H). The flow channels were sealed at the upper part with 0.2-μm filters (Sarstedt) (Figure 2I). The perfusion chambers consisted of six silicone cups (Figure 2J) that were introduced in the flow channels of the bioreactor main body and connected by pairs through silicone inlets and tubing (Figure 2K) at the bottom part. The silicone cups were made of two assembled parts (upper (red) and bottom (blue)) forming the chamber between grids (arrow in Figure 2J). The bioreactor main body was then placed on a stand (Figure 2L).

Since in the mini-Flopper, each of the three flow channels had two silicone cups, one or two scaffolds could be placed per flow channel (maximum of six scaffolds in total). The scaffolds were inserted between the grids by unclipping the middle and the bottom part (Figure 2C,D). Medium could be added and removed with pipettes by unclipping the top and the middle part (Figure 2B,C). To induce perfusion flow in each channel, a syringe pump outlet was attached to one of the filters in the upper part (asterisks in Figure 2A), while the other filter was left at atmospheric pressure. The syringe pump induced pressure differences that pushed/pulled the medium in each pair of flow channels interconnected with the inlets and tubing at the bottom part.

The upper part (Figure 2B), which has six ULN 1/4″–28 threadings, the middle part (Figure 2C), and the bottom part (Figure 2D) of the bioreactor main body were 3D-printed using two autoclavable
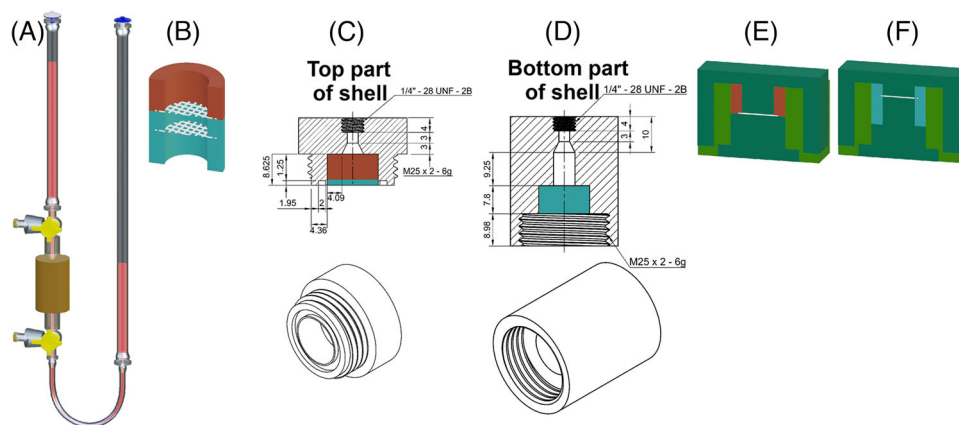
FIGURE 1 Components of the macro-Flopper bioreactor. (A) Assembled macro-Flopper bioreactor with the new perfusion chamber colored in brown. Medium is simulated in red. (B) Cross-section of the 8-mm-diameter macro-Flopper silicone cup (upper part in red and bottom part in blue) with integrated nylon grids (white). (C, D) Technical drawings to design the (C) upper and the (D) bottom parts of the outer shell that protects the silicone cup in the macro-Flopper bioreactor. (E, F) Polylactic acid (PLA) molds used to generate the (E) upper and (F) bottom parts of the silicone cup in the macro-Flopper bioreactor
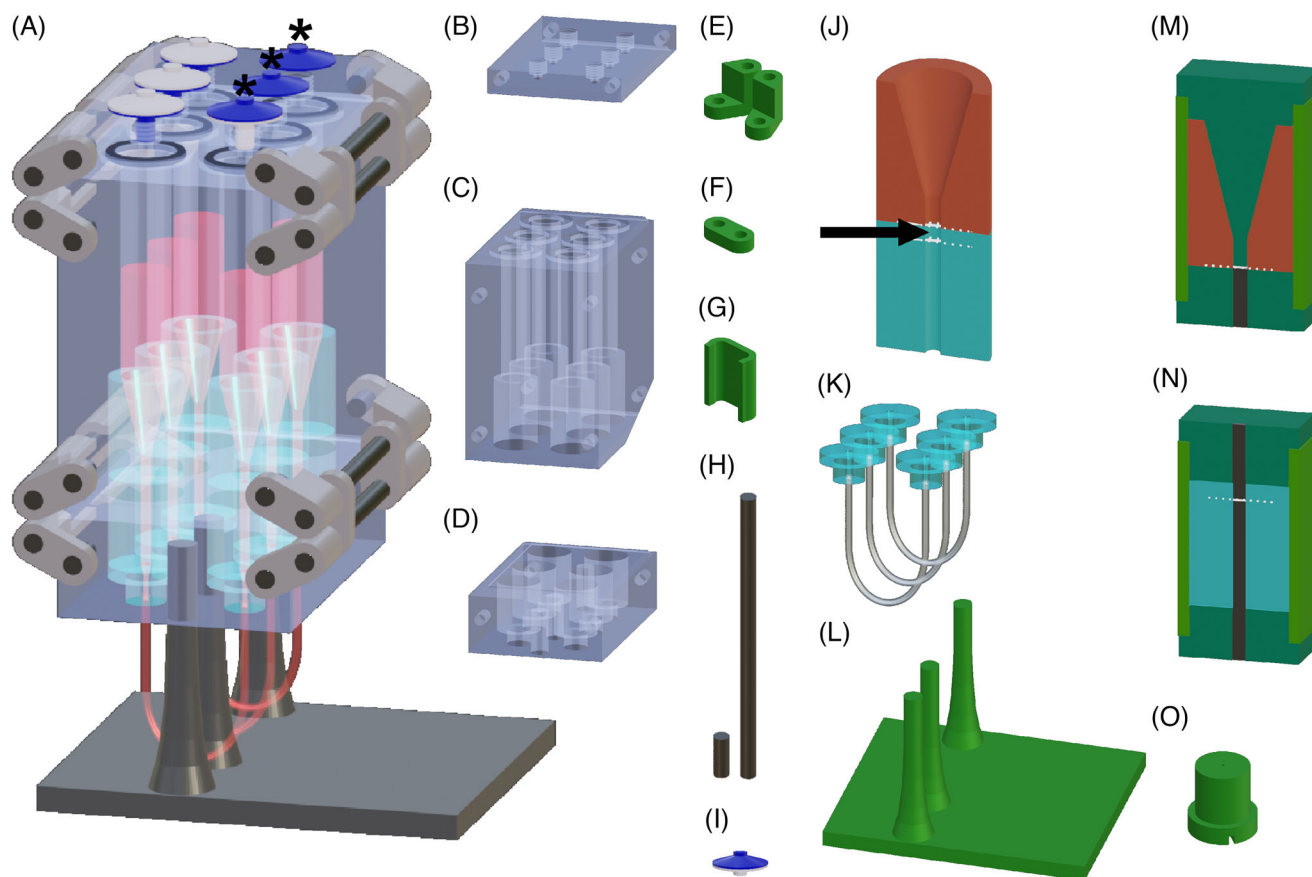

FIGURE 2 Components of the mini-Flopper bioreactor. (A) Assembled mini-Flopper bioreactor with simulated medium in the flow channels (red). (B) Upper (C) middle and (D) bottom parts of the bioreactor main body. Connectors (E), hinges (F), clippers (G), and steel rods (H) used to fix the three main parts of the mini-Flopper. (I) 0.2-μm-filters seal the flow channels at the upper part. (J) Cross-section of a 2-mm diameter silicone cup composed by an upper part (red), a bottom part (blue), and nylon grids (white) to delimitate the area containing the sample. (K) Silicone inlets with fused silicone tubing used to connect each pair of flow channels. (L) Bioreactor stand. Polylactic acid (PLA) molds used to generate the (M) upper and (N) bottom parts of the silicone cups. (O) PLA mold used to generate the silicone inlets

photopolymer resins: one as core material to build up test bodies (MED610, Stratasys Ltd., Minneapolis, USA) and the other as a water-soluble support material (SUP705, Stratasys Ltd., Minneapolis, USA). The connectors, hinges, clippers, and the stand (Figures 1L and 2E–G)) were 3D-printed using standard fused deposition modeling in PLA (green in Figure 2). The upper (red) and bottom (blue) parts of the cups were manufactured by pouring autoclavable medical-grade silicone in PLA 3D-printed molds (Figure 2M,N). These were cuboids with a 2-mm-wide slit at the side and a centered cylindrical void. The mold for the upper part of the cup (red) had a cone-shaped adapter on one side and a flat-end adapter on the other side (Figure 2M). The mold for the bottom part of the cup (blue) had two flat-end adapters on both sides (Figure 2N). The flow path space was generated using round steel rods as molds (black cylinders in Figure 2M,N). Round steel rods to generate 2×3 mm (diameter × height) chambers were used in this study. However, thanks to its modularity, the size of the perfusion chamber might be easily increased for different applications by simply using round steel rods with bigger diameters (up to 4 mm). The scaffold height was determined by the distance between the round steel rods during the manufacturing of the bottom cup. ETFE grids (white in Figure 2J,M,N) were glued with soluble water glue to the end of the round steel rods to form the meshes that held the sample in the chamber. The glue prevented the poured silicone from entering the chamber. Once the silicone was cured, the cups were washed and ready to be inserted into the bioreactor. As previously described for the macro systems, the scaffolds were also compressed in the mini-Flopper bioreactor once the chamber was sealed to reach a final size of 2×2 mm (diameter × height).

The silicone inlets were generated by pouring silicone in PLA 3D-printed molds (Figure 2O) that were inserted in the bottom part of the mini-Flopper and connected to silicone tubing (0.8 mm × 2.4 mm (ID × OD)) via 1-mm nylon monostring.

Blender 2.82 software was used to design and generate the .stl files. Cura 4.6 software was used to generate the Gcode. The autoclavable parts of the bioreactor main body were printed with a PolyJet desktop 3D printer (Objet 30 Prime, Stratasys Ltd., Minneapolis, USA). An Anycubic Mega 3D printer was used to generate all the PLA parts with a wall/bottom/top thickness of 2 mm and an infill of 20% with a step size of 100 μm.

2.3 | Computational fluid dynamics (CFD) model

A CFD simulation of the flow within each channel was performed with the commercial solver ANSYS Fluent v19.1 (ANSYS Inc., Canonsburg, PA, USA). Briefly, the .stl geometries of the three bioreactor designs (i.e., the mini-Flopper, the macro-Flopper and the U-CUP) were imported into ANSYS and discretized into tetrahedral elements to generate the 3D meshes. For each mesh, a boundary layer consisting of three prismatic elements was included, to better capture the fluid dynamics in proximity to the wall of the channel. The resulting meshes consisted of 5.8×10^5, 2.7×10^5, and 3.0×10^5 elements for the mini-Flopper, the macro-Flopper, and the U-CUP model, respectively. Plug

velocity profile and zero pressure were assigned as boundary conditions at the inlet and outlet of the channel, respectively. The no-slip condition was set at the walls. Inflow velocity and flow regimes for each bioreactor system were listed in Table S1 (Supporting Information). The medium was modeled as a homogeneous, incompressible Newtonian fluid (density $\rho = 1$ g cm^{-3}, viscosity $\mu = 1$ cP). The scaffolds were modeled as porous media[28] introducing a sink term S_i in the momentum equation, accounting for viscous and inertial loss: $S_i = - (R_V \mu v_i + 0.5 R_I \rho |v| v_i)$, where v_i is the ith velocity component, R_V is the viscous resistance and R_I is the internal resistance. When simulating the dimensions of the scaffold for each bioreactor system, the compression in the high of the scaffold upon chamber sealing was assumed. Therefore, a 8×2-mm (diameter × high) scaffold was simulated for the macro systems (U-CUP and macro-Flopper), while a 2×2-mm (diameter × high) scaffold was simulated for the mini-Flopper.

For flow at Reynolds (Re) < 1, R_V was obtained with the Kozeny–Carman equation[29]: $R_V = 150(1 - \varepsilon)^2 (\phi^2 D^2 \varepsilon^3)^{-1}$, where ε is the porosity, ϕ the sphericity, and D the average diameter of the pores; R_I was neglected. For flow at Re > 1, R_V was obtained as the inverse of the absolute permeability $R_V = - v(\mu \nabla p)^{-1}$, while R_I was defined through the Ergun equation[30]: $R_I = 1.75 L(1 - \varepsilon)(\phi D \varepsilon^3)^{-1}$. The terms in the equations were obtained from image processing, when possible, or literature. L is the width of the scaffold, equal to 2 mm. The porosity ε, defined as the void to total volume ratio of the scaffold, was computed processing micro-computed tomography (μCT) scans. Briefly, the Otsu thresholding algorithm was used to identify the void fraction of volume in each slice. The porosity was evaluated on each slice. The average porosity overall (0.9) was used as medium porosity in the simulations. Sphericity ϕ was set equal to 0.85, according to Perry's Chemical Engineers Handbook. Average diameter of the pores was estimated from μCT by calculating in ImageJ the number and the area (A) of the pores on each slice; the diameter of each pore was approximated as $D = \sqrt{(4A/\pi)}$.

2.4 | Micro-computed tomography (μCT)

μCT scans of the Zimmer Collagen Patch (Zimmer Biomet, cat# 0101Z) scaffolds were acquired using a SkyScan 1275 (Bruker) with 0.5-mm aluminum filtered X-rays (voltage 35 kV; current 350 μA). Transmission images were acquired during a 360° rotational scan with an incremental rotation step size of 0.25 grades. 3D reconstructions were made using a modified Feldkamp algorithm at an isotropic voxel size of 5 μm in NRecon software. ImageJ software (Fiji) was then used to calculate the thresholds in the resulting image stacks and determine the void to total ratio (ε, porosity).

2.5 | Cell seeding and culture in bioreactors

SVF cells, isolated from human liposuctions as previously described,[7] were seeded under perfusion on collagen type I-based scaffolds crosslinked with elastin (Zimmer Collagen Patch; Zimmer Biomet, cat#

0101Z) at a cell density of 10^4 cells mm^{-3} in each bioreactor model. The perfusion flow contributed to distribute the cells in the whole scaffold volume. For the macro-Flopper and U-CUP systems, scaffolds with 8-mm diameter and 3-mm high were seeded with $1.5*10^6$ SVF cells at a superficial speed of 1000 μm s^{-1} (3 ml min^{-1}) for 32 h. For the mini-Flopper system, six scaffolds with 2-mm diameter and 3-mm high were seeded with $9.4*10^4$ SVF cells at a superficial speed of 100 μm s^{-1} (0.029 ml min^{-1}) for 32 h. The superficial speed was reduced in the mini-Flopper to maintain the shear stress in the same range as the macro systems. It was estimated by scaling down the speed for the macro-Flopper and U-CUP systems according to the ratio of the flow channels diameters in the different systems.

Cells were seeded and cultured in pro-angiogenic complete medium for 8 days (AM), consisting of α-Minimum Essential Medium (MEM) (Gibco; cat# 22571-020) with 10% fetal bovine serum (FBS) (Gibco; cat# 10270-106), 1% HEPES (1 M) (Gibco; cat# 15630-056), 1% sodium pyruvate (100 mM) (Gibco; cat# 11360-039), 1% of Penicillin-Streptomycin-Glutamine (100X) (Gibco; cat# 10378-16) and 5 ng ml^{-1} fibroblast growth factor-2 (R&D system; cat# 233-FB). While macro-Flopper and U-CUP bioreactors were loaded with 8 ml of AM, each flow channel of the mini-Flopper system was loaded with 1 ml of AM. Therefore, the ratio between cells seeded and volume of medium was also similar between the three bioreactor models ($188*10^3$ cells ml^{-1}). After 32 h, the superficial velocity was lowered to 100 μm s^{-1} (0.3 ml min^{-1}) in the larger devices (macro-Flopper and U-CUP bioreactors) and 10 μm s^{-1} (0.0029 ml min^{-1}) for the mini-Flopper bioreactors. The medium was changed every third day. All bioreactors were kept in a humidified 37°C incubator with 5% CO_2 during the entire culture, except during the medium changes. The perfusion was established with syringe pumps (HARVARD apparatus PHD 2000 programmable) displacing air at one side of each flow channel.

After 8 days of culture, the tissues were digested for 1 h under perfusion with 0.3% collagenase II (Thermofischer; cat# 17101015) solution. Subsequently, cellularity was measured, and cell suspensions were split for flow-activated cell sorting (FACS) and Q-PCR analyses.

2.6 | Flow-activated cell sorting (FACS)

Cells were stained for 45 min at 4°C with the following antihuman antibodies diluted in PBS with 2% FBS and 2.5-mM filtered EDTA (FACS buffer) (Sigma; cat# 139-33-3): PerCP-Cy5.5 anti-CD45 (BD Biosciences; cat# 563429), APC-Cy7 anti-CD31 (BD Biosciences; cat# 563653), PE-Cy7 anti-CD146 (BioLegend; cat# 342009), and APC anti-CD90 (BD Biosciences cat# 559869). Stained cells were acquired using a LSR II FORTESSA SORP (BD Biosciences) cell analyzer. The analyses were performed using FlowJo 10.7.1.

2.7 | Immunofluorescence staining

Tissues harvested from bioreactor systems were fixed in 4% PFA and embedded in paraffin. Five micrometers sections were obtained using a microtome (Microm, HM430, Thermo Scientific). For DAPI-Phalloidin staining, sections were rehydrated and washed twice in PBS. Samples were permeabilize with 0.1% Triton X-100 for 10 min. After a wash in PBS, samples were incubated with Alexa Fluor 488 phalloidin (Invitrogen; cat# A12379) for 1 h. Samples were then washed in PBS and incubated with DAPI for 10 min. Finally, samples were mounted using Fluoromount Aqueous Mounting Medium (Sigma; cat# F4680) and acquired using a Nikon AXR confocal microscope.

2.8 | Q-PCR

Cells were resuspended in RNA lysis buffer and stored at −80°C until analysis. RNA extraction was performed using the Quick-RNA MiniPrep (Zymoresearch; cat# R1055) according to manufacturer instructions. SuperScript III Reverse Transcriptase (Invitrogen cat# 18080044) with random primers (Promega; cat# C1181) was used to retrotranscribe the RNA into cDNA. Real-time PCR (Q-PCR) was performed using TaqMan Universal PCR Master Mix (Applied Biosystems; cat# 4305719) in combination with the following "Assay on demand" TaqMan probes (Thermofisher): *MKI67* (Hs01032443), *MMP13* (Hs00233992), *COL1A1* (Hs00164004), *VCAM1* (Hs01003372), and *VWF* (Hs01109446). Ninety-six-well plates were acquired using the ABIPrism 77000 Sequence Detection System (Perkin Elmer/Applied Biosystem, Rotkreuz, Switzerland). Gene expression values were normalized to *GAPDH* (Hs02786624_g1) expression.

2.9 | Statistical analysis and reproducibility

The total cell number and composition of the different cell populations were determined using a Neubauer chamber and FACS, respectively. The compared groups were set similarly in all procedures. Results were scored blindly. Data showed in figures were means $\pm$ standard deviation (SD); "n" values were indicated in the figure legends. Parametric one-way ANOVA and Tukey comparison were used for multiple group comparisons. The data met the assumptions of the tests. Significant statistical differences between groups were indicated as: $^*p < 0.05$; $^{**}p < 0.01$; $^{***}p < 0.001$. Statistical analyses and graphics were carried out with GraphPad Prism software versions 5 and 9.

3 | RESULTS

3.1 | Flopper bioreactors show homogenous flow speed, pressure, and shear stress throughout the perfused scaffolds

We took advantage of computational fluid dynamics (CFD) modeling to evaluate the perfusion flow within the different bioreactor systems. Based on the μCT analysis, the scaffolds were simulated with a porosity of 0.9. Cross-sections of the velocity maps showed irregular flow speeds at the edges of the perfusion chamber of the U-CUP model;
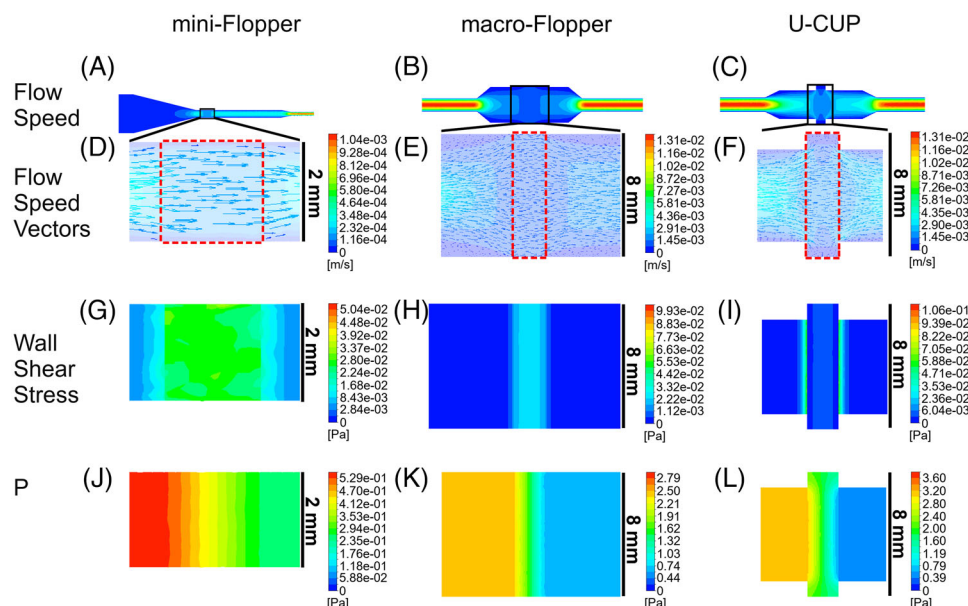
FIGURE 3 Computational flow dynamics modeling of the mini-Flopper, macro-Flopper, and U-CUP bioreactors. Color contour-maps representing the cross-section of (A–C) the flow velocity profile, (D–F) the velocity vector direction profile, (G–I) the wall shear stress, and (J–L) the pressure (indicated as "P") profile in the flow channel (including the scaffold; red-dotted box) of each bioreactor model

however, the flow speed was homogenous in the whole perfusion chamber of the mini- and macro-Flopper devices and reduced flow was observed only very close to the border of the chamber (Figure 3A–C). The visualization of the flow velocity vectors revealed straight and parallel flow in the mini- and macro-Flopper bioreactors (Figure 3D–F).

We next evaluated the wall shear stress. The results of the simulations showed uniform distribution for both mini- and macro-Flopper bioreactors, with values around $3*10^{-2}$ and $2.65*10^{-3}$ Pa, respectively. As for the flow speed, the wall shear stress was only slightly reduced very close to the borders of the chamber (Figure 3G,H). In the U-CUP system, the wall shear stress oscillated between $6*10^{-3}$ and $6*10^{-2}$ Pa (Figure 3I).

Pressure maps showed that the short-axis pressure-drop distribution was constant along the scaffold length only in the Flopper bioreactors (Figure 3J–L).

3.2 | The mini-Flopper bioreactor offers efficient cell maintenance during 3D culture

To provide a proof-of-principle of the functionality of the new bioreactor models, we assessed their capacity to support 3D cell culture, using the U-CUP bioreactor as reference. We designed an experimental setup for engineering endothelialized stromal tissues using SVF cells isolated from the adipose tissue of a patient. $1.5*10^6$ SVF cells were seeded on 150 mm³ (8-mm diameter and 3-mm high) collagen scaffolds (Zimmer Collagen Patch) and cultured for 8 days in pro-angiogenic medium within the U-CUP and macro-Flopper bioreactors. $9.4*10^4$ SVF cells were seeded on each of the 9.4 mm³ (2-mm diameter and 3-mm high) collagen scaffolds of the mini-Flopper bioreactor. At the end of the culture, samples were enzymatically digested and processed for FACS or Q-PCR analyses, as described below (Figure 4). We first measured the ratio between the number of cells harvested at the end of the culture (day 8) and number of cells seeded (day 0) in the different systems. This ratio was similar (around 1.5) for the macro-Flopper and U-CUP bioreactors and higher (2.1) for the mini-Flopper bioreactor (Figure 5A). Interestingly, the increased ratio in the mini-Flopper bioreactor was not accompanied by increased expression of the cell proliferation marker *MKI67* (Figure 5B) nor in cell morphology as revealed by DAPI/Phalloidin staining (Figure 5C–E). Altogether, our results suggest a better cell maintenance in the mini-Flopper system.

3.3 | Stromal tissue niches engineered in optimized Flopper bioreactors might be enriched in vascular cells

We next investigated by FACS the presence of endothelial (CD45⁻CD31⁺CD146⁻) cells, pericytes (CD45⁻CD31⁻CD146⁺) and mesenchymal stromal cells (CD45⁻CD31⁻CD146⁻CD90⁺) in the stromal tissues engineered within the three bioreactor systems (mini-Flopper, macro-Flopper, and U-CUP). Interestingly, the percentages of endothelial cells and pericytes in the Flopper systems (both mini and macro) were significantly higher than in the U-CUP model (Figure 6A,B), whereas the mesenchymal stromal cell (CD45⁻CD31⁻CD146⁻CD90⁺) compartment was comparable in all systems (Figure 6C). At gene expression level, von Willebrand factor (*VWF*), an endothelial cell marker, and vascular cell adhesion protein 1 (*VCAM1*) tended to be upregulated in the Flopper models, though to a reduced extent (Figure 6D,E). Finally, in order to evaluate the
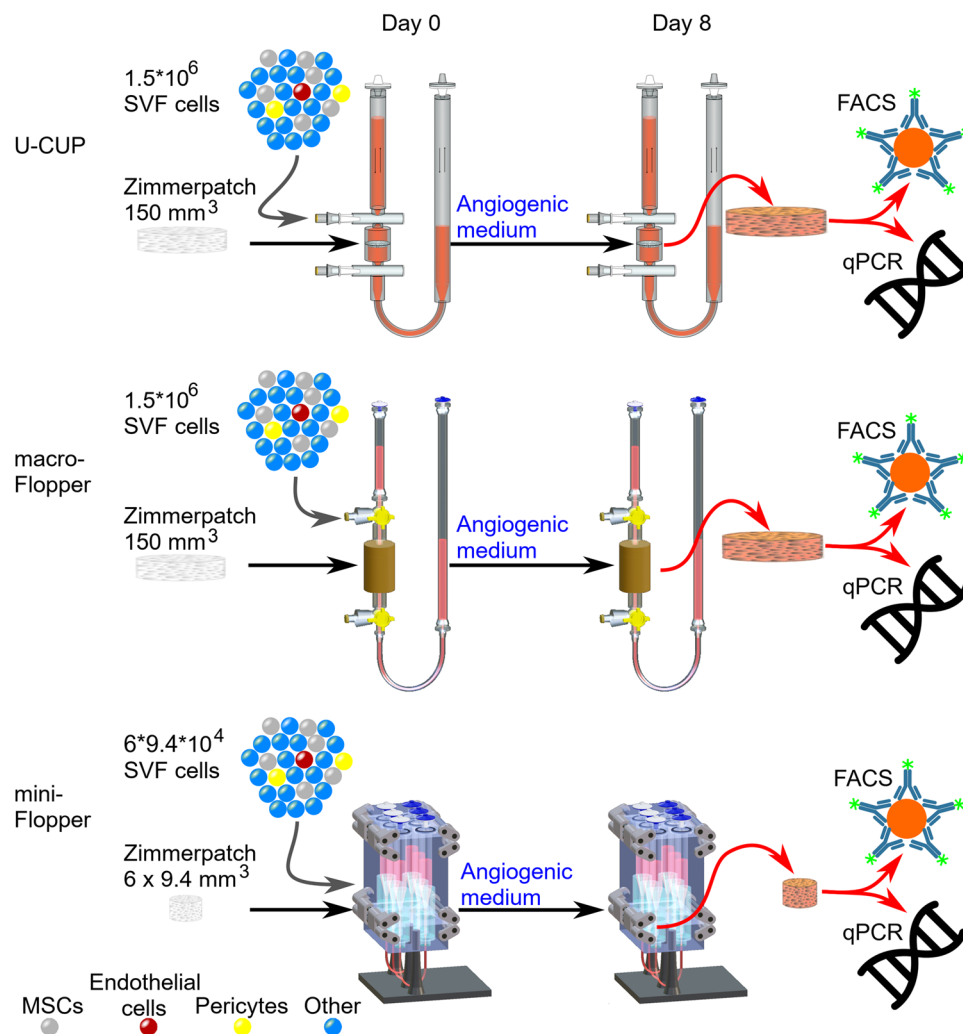
FIGURE 4 Experimental setup illustrating the protocol to engineer endothelialized stromal tissues using the three bioreactor models. Stromal vascular fraction (SVF) cells, including vascular and mesenchymal cells, were seeded on collagen scaffolds (Zimmer Collagen Patch) and cultured for 8 days in pro-angiogenic medium. At final analysis, tissues were digested and processed for flow-activated cell sorting (FACS) and gene expression (Q-PCR) analyses.

extracellular matrices generated within the bioreactor models and their remodeling activity, we measured, respectively, the expression of genes such as Collagen 1 (*COL1A1*) and Matrix Metalloproteinase 13 (*MMP13*). Both genes were highly expressed in the stromal tissues generated in the mini-Flopper bioreactor (Figure 6F,G), suggesting the presence of abundant extracellular matrix and high remodeling with the optimized flow. Taken together, these preliminary biological assays suggest that Flopper bioreactors favor the maintenance and/or expansion of cellular elements of stromal tissues.

4 | DISCUSSION AND CONCLUSIONS

Most perfusion bioreactors apply nonuniform flow and shear stress to the biological material because of the geometry of the sample chamber and/or flow channel. Acute expansions or nonrotationally symmetrical geometries tend to generate irregular flow speed areas in the periph-

ery of the sample chamber.[27] This implies that adjusting the medium flow to an average condition results in some sample areas being exposed to little and others to excessive flow and shear stress, which may affect cell proliferation and differentiation.[31,32] To circumvent this limitation, we first created a new bioreactor chamber (by designing new adapters) and ensembled it to the U-CUP tubing to generate a macro-scale flow-optimized perfusion bioreactor (macro-Flopper). This new bioreactor model ensured a homogenous and parallel flow at the peripheral areas of the perfusion chamber, even when filled with a scaffold material.

To adapt the Flopper system to medium throughput assays, we then designed and manufactured a miniaturized bioreactor system (mini-Flopper) that allows the 3D culture of small tissues (6–115 mm³) with minimal medium consumption (750 μl per flow channel). Through in silico CFD modeling, we showed that the design of the perfusion chamber in the Flopper bioreactors guarantees uniform flow speed, pressure, and shear stress throughout the sample.
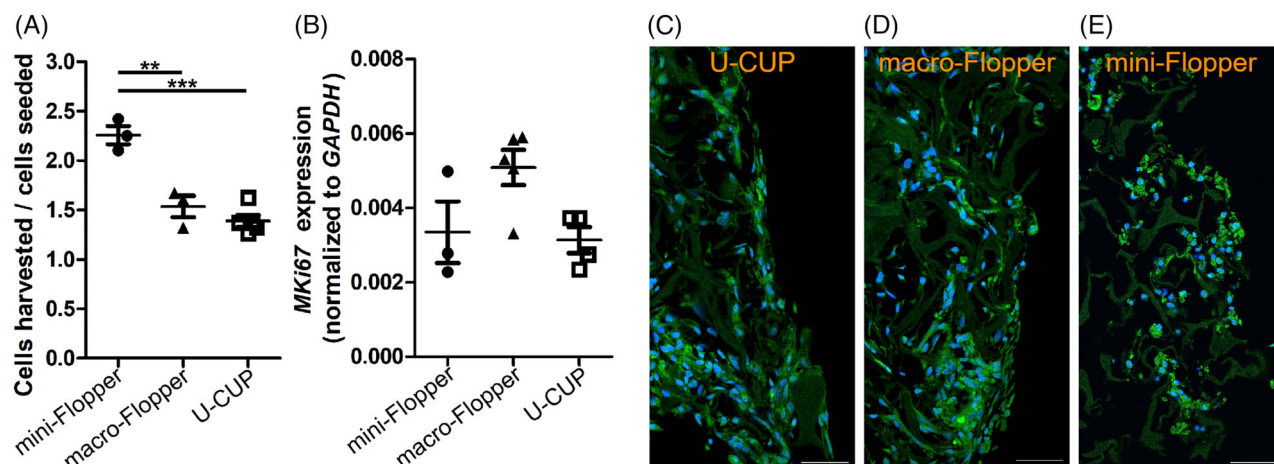
FIGURE 5 Cell maintenance was higher in the mini-Flopper bioreactor. (A) Ratio between the number of cells harvested at the end of the culture and the number of cells seeded at day 0. (B) Gene expression of the proliferation marker MKI67 in the harvested cells at the end of the culture. DAPI (blue)-Phalloidin (green) staining in the stromal tissues engineered within the (C) U-CUP, (D) macro-Flopper, and (E) mini-Flopper bioreactors. Scale bar, 50 μm. Data are plotted as means ± standard deviations; $n = 3$–6; **$p < 0.01$, ***$p < 0.001$. One-way ANOVA with Tukey's multiple comparison tests

To provide a proof-of-principle of the functionality of the Flopper bioreactors to engineer 3D tissues in vitro, we assessed their capacity to generate endothelialized stromal tissues using human adipose tissue-derived SVF cells using the U-CUP system as reference. Although previous reports have largely demonstrated that perfusion flow enhances cell proliferation in 3D constructs,[33,34] we did not detect an increase in the proliferative maker MKI67 in cells cultured in the Flopper bioreactors in comparison to the U-CUP system, suggesting that flow optimization at the edges of the perfusion chamber has little impact on cell proliferation. The fact that cell maintenance was significantly higher in the mini-Flopper than in the macro-Flopper might indicate some size-dependent effects that require further investigations. One possibility is that the lack of steep angles and transitions between valves and tubing in the design of the mini-Flopper system reduces cell adhesion to these parts, allowing better cell maintenance in the engineered tissues. In comparison to the U-CUP, Flopper bioreactors allowed the generation of engineered angiogenic tissues enriched in endothelial cells and pericytes, and promoted the expression of vascular-related genes. Interestingly, Flopper bioreactors also showed higher average shear stress values, which can directly promote endothelial cell differentiation.[35,36] Indeed high shear stress levels were shown to stimulate vascular cells differentiation and VEGF secretion by human MSCs.[37] Finally, engineered tissues from mini-Flopper bioreactors exhibited higher expression levels of *COL1A1* and *MMP13*, suggesting increased matrix production and remodeling upon flow optimization as previously described.[38]

In past years, different perfusion bioreactor systems have been developed taking into consideration the perfusion chamber geometry and the location of the scaffold within the chamber in an effort to achieve efficient and homogeneous cell seeding and distribution.[39–41] In line with our study, a bioreactor with conical diffusor geometry for the medium inlet and outlet ports (lacking steep angles) was shown to allow more homogeneous seeding of adipose derived cells than

the cylindrical shape. However, even with the conical connectors, this model has a cylindrical perfusion chamber with acute expansions very similar to those present in the U-CUP model.[42] Gabetti et al. demonstrated through CFD simulations that a conical chamber geometry very similar to the one of Flopper bioreactors avoid the formation of flow recirculation regions, which were observed in a cylindrical geometry chamber with acute expansions. Moreover, the flow velocity profile was more uniform, and low or null velocities were only present in regions close to the walls of the chamber.[43] Our results confirm these findings and further demonstrate that flow optimization at these locations in the Flopper bioreactors has an impact on global cell maintenance and differentiation. A similar chamber design was also shown to promote hMSC proliferation and differentiation and better recapitulated bone metastatic prostate cancer cell behavior.[44]

Whilst some perfusion bioreactors with the optimized flow have been proposed to engineer large bone, cartilage, or cardiac grafts,[45–47] there are limited options to generate tissues at mini-scale. Another miniaturized perfusion bioreactor similar to our mini-Flopper system was previously engineered allowing the culture of eight independent samples in parallel under physiological shear stress and hydrostatic pressures,[48] which was then assessed to generate osteogenic tissues from mesenchymal stem cells.[49] However, this bioreactor could be only operated in a big and specialized incubator system. Our miniaturized models are placed in conventional incubators and connected to external programmable syringe pumps, reducing drastically the space required. Other multichambered small-scale perfusion bioreactors showing similar characteristics than ours were also proposed to generate 3D cell constructs in hydrogel,[50] and to study the osteogenic commitment of stem cells on 3D chitosan-graphene templates.[51]

Thanks to its simple and modular design, the mini-Flopper bioreactor could be further miniaturized and/or optimized for higher-throughput drug testing assays in the context of personalized medicine,
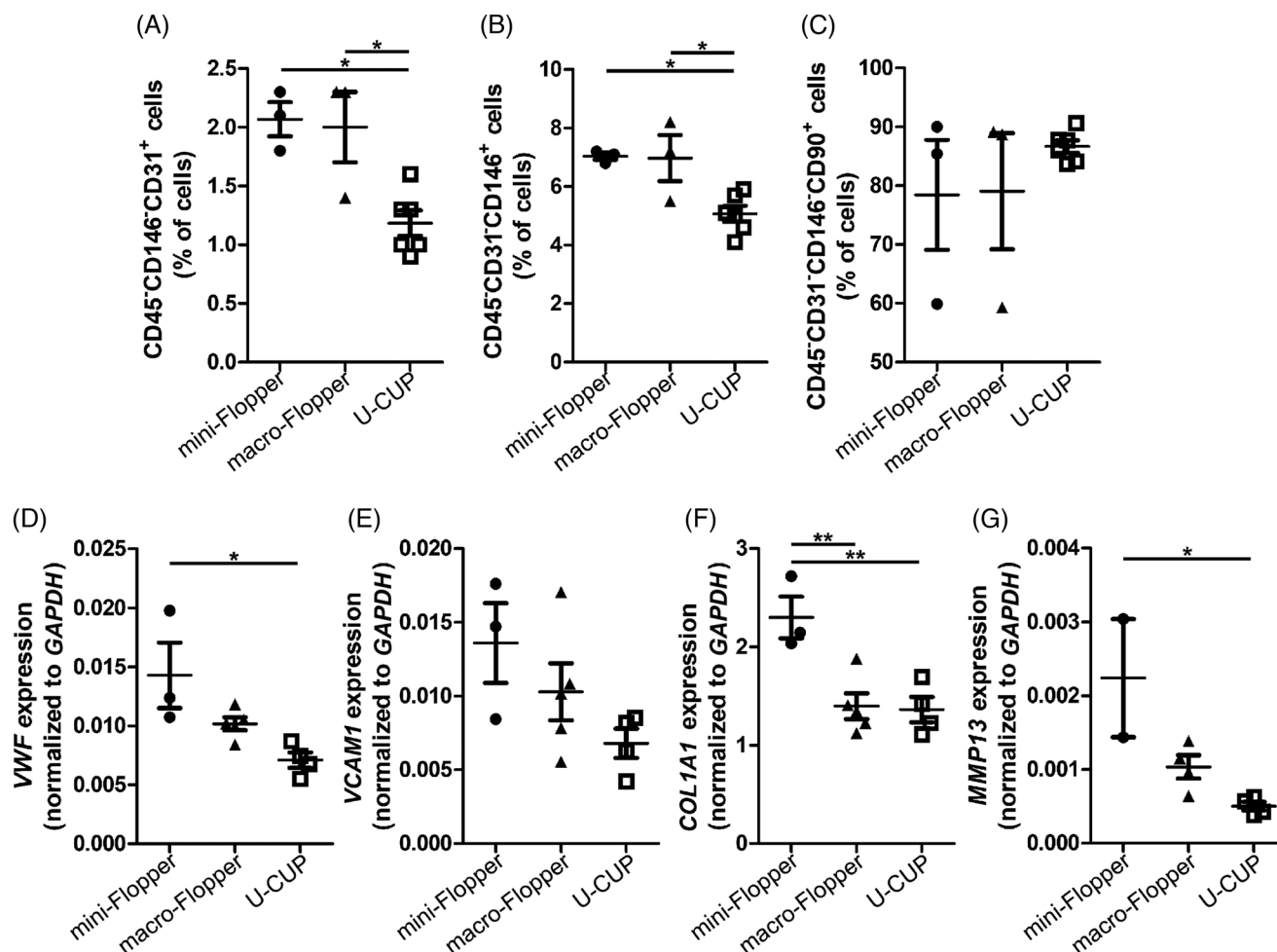
FIGURE 6 Flopper bioreactors enriched engineered stromal tissues in endothelial cells and pericytes. (A–C) Flow cytometry data showing the abundance of (A) CD45−CD31+CD146− endothelial cells, (B) CD45−CD31−CD146+ pericytes, and (C) CD45−CD31−CD146−CD90+ stromal cells in the tissues engineered within the different bioreactor models after 8 days in culture. (D–G) Gene expression of Von Willebrand factor (VWF), vascular cell adhesion molecule 1 (VCAM1), collagen 1 (COL1A1), and Matrix Metalloproteinase 13 (MMP13) in the engineered tissues at the end of the culture (day 8). Data are plotted as means ± standard deviations; $n = 2$–6; $^*p < 0.05$, $^{**}p < 0.01$. One-way ANOVA with Tukey's multiple comparison tests

where the amount of material is limited and several different conditions may need to be tested.

AUTHOR CONTRIBUTIONS

Conceptualization: Gordian Born, M. Adelaide Asnaghi, Manuele G. Muraro, Ivan Martin and Andrés García-García. *Data curation*: Gordian Born and Andrés García-García. *Formal analysis*: Gordian Born and Andrés García-García. *Investigation*: Gordian Born, Evelia Plantier, and Andrés García-García. *Methodology*: Gordian Born, Evelia Plantier, Guido Nannini, Alessandro Caimi, and Andrea Mazzoleni. *Writing—original draft*: Gordian Born, Guido Nannini, Alessandro Caimi, M. Adelaide Asnaghi, Manuele G. Muraro Arnaud Scherberich, Ivan Martin and Andrés García-García. *Software*: Guido Nannini and Alessandro Caimi. *Supervision*: Arnaud Scherberich, Ivan Martin and Andrés García-García. *Writing—review & editing*: Ivan Martin and Andrés García-García.

ACKNOWLEDGMENTS

CONFLICT OF INTEREST

The author declares that there is no conflict of interest.

DATA AVAILABILITY STATEMENT

The data that support the findings of this study and files to generate the 3D-printed components of the bioreactors are available from the corresponding author upon reasonable request.

ORCID

Andrés García-García https://orcid.org/0000-0002-8797-649X

REFERENCES

1. Gaspar, D. A., Gomide, V., & Monteiro, F. J. (2012). The role of perfusion bioreactors in bone tissue engineering. *Biomatter*, 2, 167–175. PMID: 23507883.

2. Martin, I., Wendt, D., & Heberer, M. (2004). The role of bioreactors in tissue engineering. *Trends in Biotechnology*, 22, 80–86. PMID: 14757042.

3. Wendt, D., Marsano, A., Jakob, M., Heberer, M., & Martin, I. (2003). Oscillating perfusion of cell suspensions through three-dimensional scaffolds enhances cell seeding efficiency and uniformity. *Biotechnology and Bioengineering*, 84, 205–214. PMID: 12966577.

4. Wendt, D., Stroebel, S., Jakob, M., John, G. T., & Martin, I. (2006). Uniform tissues engineered by seeding and culturing cells in 3D scaffolds under perfusion at defined oxygen tensions. *Biorheology*, 43, 481–488. PMID: 16912419.

5. Braccini, A., Wendt, D., Jaquiery, C., Jakob, M., Heberer, M., Kenins, L., Wodnar-Filipowicz, A., Quarto, R., & Martin, I. (2005). Three dimensional perfusion culture of human bone marrow cells and generation of osteoinductive grafts. *Stem Cells*, 23, 1066–1072. PMID: 16002780.

6. Scherberich, A., Galli, R., Jaquiery, C., Farhadi, J., & Martin, I. (2007). Three dimensional perfusion culture of human adipose tissue derived endothelial and osteoblastic progenitors generates osteogenic constructs with intrinsic vascularization capacity. *Stem Cells*, 25, 1823–1829. PMID: 17446558.

7. Guven, S., Mehrkens, A., Saxer, F., Schaefer, D. J., Martinetti, R., Martin, I., & Scherberich, A. (2011). Engineering of large osteogenic grafts with rapid engraftment capacity using mesenchymal and endothelial progenitors from human adipose tissue. *Biomaterials*, 32, 5801–5809. PMID: 21605897.

8. Ismail, T., Osinga, R., Todorov, A., Jr., Haumer, A., Tchang, L. A., Epple, C., Allafi, N., Menzi, N., Largo, R. D., Kaempfen, A., Martin, I., Schaefer, D. J., & Scherberich, A. (2017). Engineered, axially-vascularized osteogenic grafts from human adipose-derived cells to treat avascular necrosis of bone in a rat model. *Acta Biomaterialia*, 63, 236–245. PMID: 28893630.

9. Cerino, G., Gaudiello, E., Muraro, M. G., Eckstein, F., Martin, I., Scherberich, A., & Marsano, A. (2017). Engineering of an angiogenic niche by perfusion culture of adipose-derived stromal vascular fraction cells. *Scientific Reports*, 7, 14252. PMID: 29079730.

10. Santoro, R., Olivares, A. L., Brans, G., Wirz, D., Longinotti, C., Lacroix, D., Martin, I., & Wendt, D. (2010). Bioreactor based engineering of large-scale human cartilage grafts for joint resurfacing. *Biomaterials*, 31, 8946–8952. PMID: 20800280.

11. Vukasovic, A., Asnaghi, M. A., Kostesic, P., Quasnichka, H., Cozzolino, C., Pusic, M., Hails, L., Trainor, N., Krause, C., Figallo, E., Filardo, G., Kon, E., Wixmerten, A., Maticic, D., Pellegrini, G., Kafienah, W., Hudetz, D., Smith, T., Martin, I., … Ivkovic, A. (2019). Bioreactor manufactured cartilage grafts repair acute and chronic osteochondral defects in large animal studies. *Cell Proliferation*, 52, e12653. PMID: 31489992.

12. Papadimitropoulos, A., Scherberich, A., Guven, S., Theilgaard, N., Crooijmans, H. J., Santini, F., Scheffler, K., Zallone, A., & Martin, I. (2011). A 3D in vitro bone organ model using human progenitor cells. *European Cells & Materials [Electronic Resource]*, 21, 445–458. discussion 458. PMID: 21604244.

13. Bourgine, P. E., Klein, T., Paczulla, A. M., Shimizu, T., Kunz, L., Kokkaliaris, K. D., Coutu, D. L., Lengerke, C., Skoda, R., Schroeder, T., & Martin, I. (2018). In vitro biomimetic engineering of a human hematopoietic niche with functional properties. *Proceedings of the Natlional Academy of Sciences of the United States of America*, 115, E5688–E5695. PMID: 29866839.

14. Garcia-Garcia, A., Klein, T., Born, G., Hilpert, M., Scherberich, A., Lengerke, C., Skoda, R. C., Bourgine, P. E., & Martin, I. (2021). Cultur-

ing patient-derived malignant hematopoietic stem cells in engineered and fully humanized 3D niches. *PNAS*, 118, e2114227118.

15. Born, G., Nikolova, M., Scherberich, A., Treutlein, B., García-García, A., & Martin, I. (2021). Engineering of fully humanized and vascularized 3D bone marrow niches sustaining undifferentiated human cord blood hematopoietic stem and progenitor cells. *Journal of Tissue Engineering*, 12, 20417314211044855. PMID: 34616539.

16. Hirt, C., Papadimitropoulos, A., Muraro, M. G., Mele, V., Panopoulos, E., Cremonesi, E., Ivanek, R., Schultz-Thater, E., Droeser, R. A., Mengus, C., Heberer, M., Oertli, D., Iezzi, G., Zajac, P., Eppenberger-Castori, S., Tornillo, L., Terracciano, L., Martin, I., & Spagnoli, G. C. (2015). Bioreactor-engineered cancer tissue-like structures mimic phenotypes, gene expression profiles and drug resistance patterns observed in vivo. *Biomaterials*, 62, 138–146. PMID: 26051518.

17. Manfredonia, C., Muraro, M. G., Hirt, C., Mele, V., Governa, V., Papadimitropoulos, A., Däster, S., Soysal, S. D., Droeser, R. A., Mechera, R., Oertli, D., Rosso, R., Bolli, M., Zettl, A., Terracciano, L. M., Spagnoli, G. C., Martin, I., & Iezzi, G. (2019). Maintenance of primary human colorectal cancer microenvironment using a perfusion bioreactor based 3D culture system. *Advanced Biosystems*, 3, e1800300. PMID: 32627426.

18. Cerino, G., Gaudiello, E., Grussenmeyer, T., Melly, L., Massai, D., Banfi, A., Martin, I., Eckstein, F., Grapow, M., & Marsano, A. (2016). Three dimensional multi-cellular muscle-like tissue engineering in perfusion-based bioreactors. *Biotechnology and Bioengineering*, 113, 226–236. PMID: 26126766.

19. Muraro, M. G., Muenst, S., Mele, V., Quagliata, L., Iezzi, G., Tzankov, A., Weber, W. P., Spagnoli, G. C., & Soysal, S. D. (2017). Ex-vivo assessment of drug response on breast cancer primary tissue with preserved microenvironments. *Oncoimmunology*, 6, e1331798. PMID: 28811974.

20. Foglietta, F., Spagnoli, G. C., Muraro, M. G., Ballestri, M., Guerrini, A., Ferroni, C., Aluigi, A., Sotgiu, G., & Varchi, G. (2018). Anticancer activity of paclitaxel-loaded keratin nanoparticles in two-dimensional and perfused three-dimensional breast cancer models. *International Journal of Nanomedicine*, 13, 4847–4867. PMID: 30214193.

21. Amadeo, F., Boschetti, F., Polvani, G., Banfi, C., Pesce, M., & Santoro, R. (2018). Aortic valve cell seeding into decellularized animal pericardium by perfusion-assisted bioreactor. *Journal of Tissue Engineering and Regenerative Medicine*, 12, 1481–1493. PMID: 29702745.

22. Amadeo, F., Barbuto, M., Bernava, G., Savini, N., Brioschi, M., Rizzi, S., Banfi, C., Polvani, G., & Pesce, M. (2020). Culture into perfusion-assisted bioreactor promotes valve-like tissue maturation of recellularized pericardial membrane. *Frontiers in Cardiovascular Medicine*, 7, 80. PMID: 32478099.

23. Bao, K., Papadimitropoulos, A., Akgul, B., Belibasakis, G. N., & Bostanci, N. (2015). Establishment of an oral infection model resembling the periodontal pocket in a perfusion bioreactor system. *Virulence*, 6, 265–273. PMID: 25587671.

24. Rossi, E., Guerrero, J., Aprile, P., Tocchio, A., Kappos, E. A., Gerges, I., Lenardi, C., Martin, I., & Scherberich, A. (2018). Decoration of RGD-mimetic porous scaffolds with engineered and devitalized extracellular matrix for adipose tissue regeneration. *Acta Biomaterialia*, 73, 154–166. PMID: 29684623.

25. Neutzner, A., Power, L., Durrenberger, M., Scholl, H. P. N., Meyer, P., Killer, H. E., Wendt, D., & Kohler, C. (2019). A perfusion bioreactor-based 3D model of the subarachnoid space based on a meningeal tissue construct. *Fluids Barriers CNS*, 16, 17. PMID: 31189484.

26. Asnaghi, M. A., Barthlott, T., Gullotta, F., Strusi, V., Amovilli, A., Hafen, K., Srivastava, G., Oertle, P., Toni, R., Wendt, D., Holländer, G. A., & Martin, I. (2021). Thymus extracellular matrix derived scaffolds support graft resident thymopoiesis and long term in vitro culture of adult thymic epithelial cells. *Advanced Functional Materials*, 31, 2010747. PMID: 34539304.

27. Hidalgo-Bastida, L. A., Thirunavukkarasu, S., Griffiths, S., Cartmell, S. H., & Naire, S. (2012). Modeling and design of optimal flow

perfusion bioreactors for tissue engineering applications. *Biotechnology and Bioengineering*, 109, 1095–1099. PMID: 22068720.

28. Schmid, J., Schwarz, S., Meier-Staude, R., Sudhop, S., Clausen-Schaumann, H., Schieker, M., & Huber, R. (2018). A perfusion bioreactor system for cell seeding and oxygen-controlled cultivation of three-dimensional cell cultures. *Tissue Eng Part C Methods*, 24, 585–595. PMID: 30234443.

29. Carman, P. C. (1997). Fluid flow through granular beds. *Chemical Engineering Research and Design*, 75, S32–S48.

30. Ergun, S. (1952). Fluid flow through packed columns. *Chemical Engineering Progress*, 48, 89–94.

31. Riddle, R. C., Taylor, A. F., Genetos, D. C., & Donahue, H. J. (2006). MAP kinase and calcium signaling mediate fluid flow-induced human mesenchymal stem cell proliferation. *American Journal of Physiology. Cell Physiology*, 290, C776–C784. PMID: 16267109.

32. Yamamoto, K., Sokabe, T., Watabe, T., Miyazono, K., Yamashita, J. K., Obi, S., Ohura, N., Matsushita, A., Kamiya, A., & Ando, J. (2005). Fluid shear stress induces differentiation of Flk-1-positive embryonic stem cells into vascular endothelial cells in vitro. *American Journal of Physiology. Heart and Circulatory Physiology*, 288, H1915–H1924. PMID: 15576436.

33. Santoro, M., Lamhamedi-Cherradi, S. E., Menegaz, B. A., Ludwig, J. A., & Mikos, A. G. (2015). Flow perfusion effects on three-dimensional culture and drug sensitivity of ewing sarcoma. *PNAS*, 112, 10304–10309. PMID: 26240353.

34. Kitagawa, T., Yamaoka, T., Iwase, R., & Murakami, A. (2006). Three-dimensional cell seeding and growth in radial-flow perfusion bioreactor for in vitro tissue reconstruction. *Biotechnology and Bioengineering*, 93, 947–954. PMID: 16329144.

35. Potter, C. M., Lao, K. H., Zeng, L., & Xu, Q. (2014). Role of biomechanical forces in stem cell vascular lineage differentiation. *Arteriosclerosis, Thrombosis, and Vascular Biology*, 34, 2184–2190. PMID: 25012135.

36. Kolluru, G. K., Sinha, S., Majumder, S., Muley, A., Siamwala, J. H., Gupta, R., & Chatterjee, S. (2010). Shear stress promotes nitric oxide production in endothelial cells by sub-cellular delocalization of eNOS: A basis for shear stress mediated angiogenesis. *Nitric Oxide*, 22, 304–315. PMID: 20188204.

37. Yuan, L., Sakamoto, N., Song, G., & Sato, M. (2013). High-level shear stress stimulates endothelial differentiation and VEGF secretion by human mesenchymal stem cells. *Cellular and Molecular Bioengineering*, 6, 220–229.

38. Bancroft, G. N., Sikavitsas, V. I., van den Dolder, J., Sheffield, T. L., Ambrose, C. G., Jansen, J. A., & Mikos, A. G. (2002). Fluid flow increases mineralized matrix deposition in 3D perfusion culture of marrow stromal osteoblasts in a dose-dependent manner. *PNAS*, 99, 12600–12605. PMID: 12242339.

39. Zermatten, E., Vetsch, J. R., Ruffoni, D., Hofmann, S., Müller, R., & Steinfeld, A. (2014). Micro-computed tomography based computational fluid dynamics for the determination of shear stresses in scaffolds within a perfusion bioreactor. *Annals of Biomedical Engineering*, 42, 1085–1094. PMID: 24492950.

40. Yamada, S., Yassin, M. A., Schwarz, T., Mustafa, K., & Hansmann, J. (2022). Optimization and validation of a custom-designed perfusion bioreactor for bone tissue engineering: Flow assessment and optimal culture environmental conditions. *Frontiers in Bioengineering and Biotechnology*, 10, 811942. PMID: 35402393.

41. Papantoniou, I., Guyot, Y., Sonnaert, M., Kerckhofs, G., Luyten, F. P., Geris, L., & Schrooten, J. (2014). Spatial optimization in perfusion bioreactors improves bone tissue-engineered construct quality attributes. *Biotechnology and Bioengineering*, 111, 2560–2570. PMID: 24902541.

42. Engel, N., Fechner, C., Voges, A., Ott, R., Stenzel, J., Siewert, S., Bergner, C., Khaimov, V., Liese, J., Schmitz, K. - P., Krause, B. J., & Frerich, B. (2021). An optimized 3D-printed perfusion bioreactor for homogeneous cell seeding in bone substitute scaffolds for future chairside applications. *Scientific Reports*, 11, 22228. PMID: 34782672.

43. Gabetti, S., Masante, B., Cochis, A., Putame, G., Sanginario, A., Armando, I., Fiume, E., Scalia, A. C., Daou, F., Baino, F., Salati, S., Morbiducci, U., Rimondini, L., Bignardi, C., & Massai, D. (2022). An automated 3D-printed perfusion bioreactor combinable with pulsed electromagnetic field stimulators for bone tissue investigations. *Scientific Reports*, 12, 13859. PMID: 35974079.

44. Jasuja, H., Kar, S., Katti, D. R., & Katti, K. S. (2021). Perfusion bioreactor enabled fluid-derived shear stress conditions for novel bone metastatic prostate cancer testbed. *Biofabrication*, 13, 035004.

45. Bhaskar, B., Owen, R., Bahmaee, H., Rao, P. S., & Reilly, G. C. (2018). Design and assessment of a dynamic perfusion bioreactor for large bone tissue engineering scaffolds. *Applied Biochemistry and Biotechnology*, 185, 555–563. PMID: 29235057.

46. Daly, A. C., Sathy, B. N., & Kelly, D. J. (2018). Engineering large cartilage tissues using dynamic bioreactor culture at defined oxygen conditions. *Journal of Tissue Engineering*, 9, 2041731417753718. PMID: 29399319.

47. Visone, R., Talò, G., Lopa, S., Rasponi, M., & Moretti, M. (2018). Enhancing all-in-one bioreactors by combining interstitial perfusion, electrical stimulation, on-line monitoring and testing within a single chamber for cardiac constructs. *Scientific Reports*, 8, 16944. PMID: 30446711.

48. Egger, D., Fischer, M., Clementi, A., Ribitsch, V., Hansmann, J., & Kasper, C. (2017). Development and characterization of a parallelizable perfusion bioreactor for 3D cell culture. *Bioengineering (Basel)*, 4, 51. PMID: 28952483.

49. Egger, D., Spitz, S., Fischer, M., Handschuh, S., Glösmann, M., Friemert, B., Egerbacher, M., & Kasper, C. (2017). Application of a parallelizable perfusion bioreactor for physiologic 3D cell culture. *Cells Tissues Organs*, 203, 316–326. PMID: 28291964.

50. Mendonca da Silva, J., Erro, E., Awan, M., Chalmers, S. A., Fuller, B., & Selden, C. (2020). Small-Scale fluidized bed bioreactor for long-term dynamic culture of 3D cell constructs and in vitro testing. *Frontiers in Bioengineering and Biotechnology*, 8, 895. PMID: 32974291.

51. Lovecchio, J., Gargiulo, P., Vargas Luna, J. L., Giordano, E., & Sigurjonsson, O. E. (2019). A standalone bioreactor system to deliver compressive load under perfusion flow to hBMSC-seeded 3D chitosan-graphene templates. *Scientific Reports*, 9, 16854. PMID: 31728040.

SUPPORTING INFORMATION

Additional supporting information can be found online in the Supporting Information section at the end of this article.